J. Fluid Mech. (2004), *vol.* 501, *pp.* 169–178.
DOI: 10.1017/S0022112003007444 Printed in the United Kingdom

Statistics of gravity waves obtained by direct numerical simulation

By NAOTO YOKOYAMA

Department of Physics, Graduate School of Science, Kyoto University, Kitashirakawa-oiwake-cho, Sakyo, Kyoto 606-8502, Japan

(Received 24 September 2003 and in revised form 12 November 2003)

We perform direct numerical simulations of dynamic equations of decaying gravity waves on infinite-depth water. Power-law behaviour of the wave action spectrum and structure functions of the surface elevation is obtained. These power laws agree with the prediction of the weak turbulence theory. The probability density function (p.d.f.) of the surface elevation is close to the Gaussian distribution around the mean value which seems to be consistent with the random phase approximation. However, the p.d.f. deviates weakly from the Gaussian in the tail region. This deviation is significant and can be amplified by taking the Laplacian. In addition, intermittency and breakdown of the weak turbulence theory are discussed.

1. Introduction

Studies on water wave systems that have broad-band energy spectra date back to the 1960s. Zakharov (1968) showed that the evolution of infinite-depth water waves is described by canonical equations and derived the so-called Zakharov equation. Moreover, he derived the nonlinear Schrödinger equation and examined modulational instability.

While much work has been carried out since then, the random phase approximation is the most important and useful procedure for statistics of water wave systems. With this approximation, the Zakharov equation leads to the kinetic equation (Zakharov & Filonenko 1967),

$$\frac{\partial n(\boldsymbol{k})}{\partial t} = \int \mathrm{d}\boldsymbol{k}_{123}\delta^{\boldsymbol{k}}_{0+1-2-3}\delta^{\omega}_{0+1-2-3}|T_{0,1,2,3}|^2 n_0 n_1 n_2 n_3 \left(\frac{1}{n_0}+\frac{1}{n_1}-\frac{1}{n_2}-\frac{1}{n_3}\right), \tag{1.1}$$

where $n_i = n(\boldsymbol{k}_i)$ is wave action, $\boldsymbol{k}$ is the horizontal wavenumber, $\mathrm{d}\boldsymbol{k}_{123} = \mathrm{d}\boldsymbol{k}_1\,\mathrm{d}\boldsymbol{k}_2\,\mathrm{d}\boldsymbol{k}_3$ and $T_{0,1,2,3}$ is the matrix element. The most important parts of this equation are the two δ-functions. They show that energy transfer and wave action transfer occur among the wavenumbers that satisfy the resonant relationship

$$\boldsymbol{k} + \boldsymbol{k}_1 = \boldsymbol{k}_2 + \boldsymbol{k}_3, \tag{1.2a}$$

$$\omega(\boldsymbol{k}) + \omega(\boldsymbol{k}_1) = \omega(\boldsymbol{k}_2) + \omega(\boldsymbol{k}_3), \tag{1.2b}$$

where $\omega(\boldsymbol{k}) = \sqrt{g|\boldsymbol{k}|}$ (g is the acceleration due to gravity) is the linear dispersion relation. This kinetic theory is called the weak turbulence theory. Most theoretical work on the statistics of nonlinear water wave systems (Polnikov 1994) and weather forecasts (Komen *et al.* 1994) has been based on the kinetic equation (1.1).

Similarly to the two-dimensional fully developed Navier–Stokes turbulence, the isotropic infinite-depth water wave system has two invariants, the total energy and

the total wave action, and is considered to have two quasi-equilibrium stationary states:

$$n(\boldsymbol{k}) \propto \begin{cases} |\boldsymbol{k}|^{-4} & \text{(energy cascade)}, \\ |\boldsymbol{k}|^{-23/6} & \text{(wave action cascade)}. \end{cases} \tag{1.3}$$

In the same way, the structure functions of the displacement of the wave surface, η, have a power-law behaviour. The pth structure function of the surface increments over a horizontal distance $\boldsymbol{r}$ is defined as $S_p(\boldsymbol{r}) = \langle |\eta(\boldsymbol{x}+\boldsymbol{r}) - \eta(\boldsymbol{x})|^p \rangle$, where $\langle \cdot \rangle$ means averaging over horizontal positions $\boldsymbol{x}$ and ensembles. The exponent of the power law, ζ_p, where $S_p(\boldsymbol{r}) \propto |\boldsymbol{r}|^{\zeta_p}$, is derived as follows:

$$\zeta_p = \begin{cases} 3p/4 & \text{(energy cascade)}, \\ 2p/3 & \text{(wave action cascade)}. \end{cases} \tag{1.4}$$

While the self-similarity in fully developed Navier–Stokes turbulence can be determined only by a dimensional analysis, the derivation of the law in water wave turbulence needs an additional constraint because of the excess of independent physical quantities. The kinetic equation (1.1) implies that the energy transfer and the wave action transfer are proportional to the third power of the wave action. This implication is traditionally used as the constraint. Therefore we shall try to obtain the self-similarity from the dynamic equations.

Leaving aside the success of the weak turbulence theory, much attention has been paid to the rich features of wave turbulence that cannot be obtained by the random phase approximation. Numerical studies on various wave turbulence systems with the dynamic equations have recently been made actively (e.g. Pushkarev & Zakharov 2000; Cai & McLaughlin 2000; Zakharov, Vasilyev & Dyachenko 2001; Dias, Guyenne & Zakharov 2001). Although these features originate from dynamical properties and the kinetic equation (1.1) cannot describe physical quantities in real space, few direct numerical simulations have been carried out on the infinite-depth gravity wave system (e.g. Tanaka 2001).

Onorato *et al.* (2002) obtained power-law spectra in the infinite-depth gravity wave system. The difference between their simulation and ours is the angular dependence of the spectra. They used an initial condition with cosine-squared angular dependence and we use an initial condition without angular dependence. The reason why we carried out the numerical simulation of isotropic spectra is to avoid correction for the spectra due to anisotropy: power laws are predicted not for anisotropic spectra but for isotropic ones. In fact, based on the kinetic equation (1.1), Polnikov (2001) numerically showed that the stationary spectra for the energy cascade deviate from the power-law behaviour predicted by the weak turbulence theory due to anisotropic forcing, while those for the wave action cascade do not.

In this paper, we perform direct numerical simulations for decaying infinite-depth water wave turbulence driven by an energy cascade and investigate the statistics of the wave field. The dynamic equations governing the gravity waves and the method of numerical simulation are explained in § 2. Numerical results are given in § 3. In addition, the validity of the weak turbulence theory and its breakdown are discussed in § 4.

2. The method of direct numerical simulation

In this paper we deal with three-dimensional gravity waves on infinite-depth water. When the motion is irrotational, inviscid and incompressible, it is described by

four equations: Laplace's equation with respect to the velocity potential $\phi(\boldsymbol{x}, z)$, the kinematic and dynamic boundary conditions at the free surface $z=\eta(\boldsymbol{x})$, and the boundary condition at the bottom. These are expressed as follows:

$$\left.\begin{aligned}
&\nabla^2\phi(\boldsymbol{x}, z) = 0 && \text{for } -\infty < z < \eta(\boldsymbol{x}),\\
&\frac{\partial\eta(\boldsymbol{x})}{\partial t} + (\nabla_\perp\phi(\boldsymbol{x}, z))\cdot(\nabla_\perp\eta(\boldsymbol{x})) - \frac{\partial\phi(\boldsymbol{x}, z)}{\partial z} = 0 && \text{on } z=\eta(\boldsymbol{x}),\\
&\frac{\partial\phi(\boldsymbol{x}, z)}{\partial t} + \tfrac{1}{2}(\nabla\phi(\boldsymbol{x}, z))^2 + gz = p && \text{on } z=\eta(\boldsymbol{x}),\\
&\frac{\partial\phi(\boldsymbol{x}, z)}{\partial z} \to 0 && \text{as } z\to-\infty,
\end{aligned}\right\} \tag{2.1}$$

where ∇^2 is the Laplacian and $\nabla_\perp = (\partial/\partial x, \partial/\partial y)$ is the horizontal gradient operator, p is the atmospheric pressure, and the density of water is normalized to unity. From now on, g is normalized to unity and p is set to be zero.

In terms of the surface elevation $\eta(\boldsymbol{x})$ and the surface potential $\phi^{\mathrm{s}}(\boldsymbol{x}) = \phi(\boldsymbol{x}, \eta(\boldsymbol{x}))$ we can rewrite these equations as deterministic equations up to the order of four-wave interactions:

$$\begin{aligned}
\frac{\partial\hat\eta(\boldsymbol{k})}{\partial t} &= |\boldsymbol{k}|\hat\phi^{\mathrm{s}}(\boldsymbol{k}) - \frac{1}{L}|\boldsymbol{k}|\int \mathrm{d}\boldsymbol{k}_{12}\delta^{\boldsymbol{k}}_{0-1-2}|\boldsymbol{k}_1|\hat\phi^{\mathrm{s}}_1\hat\eta_2 + \frac{1}{L}\boldsymbol{k}\cdot\int \mathrm{d}\boldsymbol{k}_{12}\delta^{\boldsymbol{k}}_{0-1-2}\boldsymbol{k}_1\hat\phi^{\mathrm{s}}_1\hat\eta_2\\
&\quad - \frac{1}{L^2}\frac{|\boldsymbol{k}|^2}{2}\int \mathrm{d}\boldsymbol{k}_{123}\delta^{\boldsymbol{k}}_{0-1-2-3}|\boldsymbol{k}_1|\hat\phi^{\mathrm{s}}_1\hat\eta_2\hat\eta_3 - \frac{1}{L^2}\frac{|\boldsymbol{k}|}{2}\int \mathrm{d}\boldsymbol{k}_{123}\delta^{\boldsymbol{k}}_{0-1-2-3}|\boldsymbol{k}_1|^2\hat\phi^{\mathrm{s}}_1\hat\eta_2\hat\eta_3\\
&\quad + \frac{1}{L^2}|\boldsymbol{k}|\int \mathrm{d}\boldsymbol{k}_{12}\delta^{\boldsymbol{k}}_{0-1-2}\hat\eta_1|\boldsymbol{k}_2|\int \mathrm{d}\boldsymbol{k}_{34}\delta^{\boldsymbol{k}}_{2-3-4}|\boldsymbol{k}_3|\hat\phi^{\mathrm{s}}_3\hat\eta_4,
\end{aligned} \tag{2.2a}$$

$$\begin{aligned}
\frac{\partial\hat\phi^{\mathrm{s}}(\boldsymbol{k})}{\partial t} &= -\hat\eta(\boldsymbol{k}) + \frac{1}{L}\frac{1}{2}\int \mathrm{d}\boldsymbol{k}_{12}\delta^{\boldsymbol{k}}_{0-1-2}(|\boldsymbol{k}_1||\boldsymbol{k}_2| + \boldsymbol{k}_1\cdot\boldsymbol{k}_2)\hat\phi^{\mathrm{s}}_1\hat\phi^{\mathrm{s}}_2\\
&\quad + \frac{1}{L^2}\int \mathrm{d}\boldsymbol{k}_{123}\delta^{\boldsymbol{k}}_{0-1-2-3}|\boldsymbol{k}_1|^2\hat\phi^{\mathrm{s}}_1|\boldsymbol{k}_2|\hat\phi^{\mathrm{s}}_2\hat\eta_3\\
&\quad - \frac{1}{L^2}\int \mathrm{d}\boldsymbol{k}_{12}\delta^{\boldsymbol{k}}_{0-1-2}|\boldsymbol{k}_1|\hat\phi^{\mathrm{s}}_1|\boldsymbol{k}_2|\int \mathrm{d}\boldsymbol{k}_{34}\delta^{\boldsymbol{k}}_{2-3-4}|\boldsymbol{k}_3|\hat\phi^{\mathrm{s}}_3\hat\eta_4,
\end{aligned} \tag{2.2b}$$

where L is the period length and $\hat\eta_i = \hat\eta(\boldsymbol{k}_i) = L^{-1}\int \mathrm{d}\boldsymbol{x}\eta(\boldsymbol{x})\exp(-\mathrm{i}\boldsymbol{k}_i\cdot\boldsymbol{x})$. Equations (2.2) are completely equivalent to (4.8), (4.9) in Krasitskii (1994) up to the order of the four-wave interactions. The advantage of using (2.2) in our numerical computation is that these equations are suitable for spectral methods using the fast Fourier transforms.

The transformation from (2.1) to (2.2) means that the three-dimensional free boundary problem is reduced to a two-dimensional boundary problem which is truncated up to the order of four-wave interactions. The truncation is commonly used but is not always acceptable since it is possible that higher-order nonlinear terms can be larger than linear or lower-order nonlinear terms. This is discussed further in § 4.

Now we introduce complex amplitude variable $b(\boldsymbol{k})$ as

$$b(\boldsymbol{k}) = \sqrt{\frac{\omega(\boldsymbol{k})}{2|\boldsymbol{k}|}}\hat\eta(\boldsymbol{k}) + \mathrm{i}\sqrt{\frac{|\boldsymbol{k}|}{2\omega(\boldsymbol{k})}}\hat\phi^{\mathrm{s}}(\boldsymbol{k}). \tag{2.3}$$

In addition we add dissipation term $-D(|\boldsymbol{k}|)b(\boldsymbol{k})$ to (2.2). Of course, this term is artificial but it is assumed that the term does not affect the dynamics in the inertial range. Then (2.2) are rewritten in one complex-variable differential-integral equation

as

$$\frac{\partial b(\boldsymbol{k})}{\partial t} = -\mathrm{i}\omega(\boldsymbol{k})b(\boldsymbol{k}) + \mathcal{N}(b(\boldsymbol{k})) - D(|\boldsymbol{k}|)b(\boldsymbol{k}), \tag{2.4}$$

where the nonlinear term $\mathcal{N}(b(\boldsymbol{k}))$ consisting of many integrals comes from the nonlinear terms of (2.2). For the dissipation term, we used the form of $D(|\boldsymbol{k}|) = \nu|\boldsymbol{k}|^{n_\mathrm{D}}$, where $n_\mathrm{D} = 16$ and $\nu \sim 6.58 \times 10^{-24}$.

We used the modified JONSWAP spectrum without directional dependence as the initial condition of the energy spectrum. The initial condition we employed was

$$|b(\boldsymbol{k})|^2 = C|\boldsymbol{k}|^{-9/2} \exp\left(-\frac{5}{4|\boldsymbol{k}|^2}\right) \gamma^{\exp(-(|\boldsymbol{k}|-k_\mathrm{P})^2/(2\sigma^2))} \exp\left(-\left(\frac{|\boldsymbol{k}|}{k_\mathrm{cutoff}}\right)^2\right), \tag{2.5}$$

where C is chosen to determine linear energy density $H_\mathrm{L} = \int \mathrm{d}\boldsymbol{k}\omega(\boldsymbol{k})|b(\boldsymbol{k})|^2$, the peak wavenumber k_P is set to be unity, $\gamma = 3.3$, and

$$\sigma = \begin{cases} 0.07 & \text{for } |\boldsymbol{k}| < k_\mathrm{P}, \\ 0.09 & \text{for } |\boldsymbol{k}| \geqslant k_\mathrm{P}. \end{cases} \tag{2.6}$$

The extra term, $\exp(-(|\boldsymbol{k}|/k_\mathrm{cutoff})^2)$, is the cutoff at large wavenumbers to avoid initial instability and we used $k_\mathrm{cutoff} = 2$. The initial phases of the $b(\boldsymbol{k})$ are given by random numbers homogeneously distributed in $[0, 2\pi)$.

With the characteristic wave amplitude $A_\mathrm{c} \sim 2\sqrt{H_\mathrm{L}}$, the mean slope of waves ε, which is one of the parameters indicating the strength of the nonlinear interaction, is estimated as $k_\mathrm{P}A_\mathrm{c}$. If H_L is too large, waves collapse everywhere and the system is not the weak turbulence regime. On the other hand, if H_L is too small, the numerical simulations are time-consuming. Therefore we must choose an appropriate H_L, and here set H_L to 5.0×10^{-3}.

We carried out this calculation with 2048^2 effective mesh points, which requires 4096^2-grid-point fast Fourier transforms since we employed the so-called '3/2 method' for de-aliasing. We integrated (2.4) by the fourth-order Runge–Kutta method with the time step $\Delta t = T_\mathrm{P}/100$; T_P is the period of the peak wavenumber k_P and is normalized to 2π. However, below $1000T_\mathrm{P}$ we used $\Delta t = T_\mathrm{P}/50$ to save computation time.

The computational domain is a doubly periodic square whose edge is 32 times as large as the wavelength of the peak wavenumber, and the wavenumbers are discretized as $\boldsymbol{k} = (m/32, n/32)$ $(-1023 \leqslant m, n \leqslant 1023)$.

At first, we expected the minimum wavenumber, 1/32 here, to be important to collect a large number of combinations of resonant quartets in numerical simulations and that we should make it as small as possible. The discretization is believed to cause frozen turbulence, in which low-wavenumber modes exchange energy without net energy transfer. In fact, Kartashova (1998) showed analytically, and Pushkarev & Zakharov (2000) numerically, that the discretization causes frozen turbulence on capillary waves, where the net energy transfer occurs among resonant trios. However, for resonant quartets it has recently been found that the minimum wavenumber is not important unless we are interested in extremely small wavenumbers. It is proved that many quartets, apart from trivial ones which do not contribute to the net energy transfer such as $\boldsymbol{k} = \boldsymbol{k}_2$ and $\boldsymbol{k}_1 = \boldsymbol{k}_3$, *exactly* satisfy the four-wave resonant condition (1.2) even in a sparsely discretized domain with a rectangular grid (Tanaka & Yokoyama 2004) irrespective of the degrees of freedom. Namely, the resonance among even-numbered waves is completely different from that among odd-numbered waves.

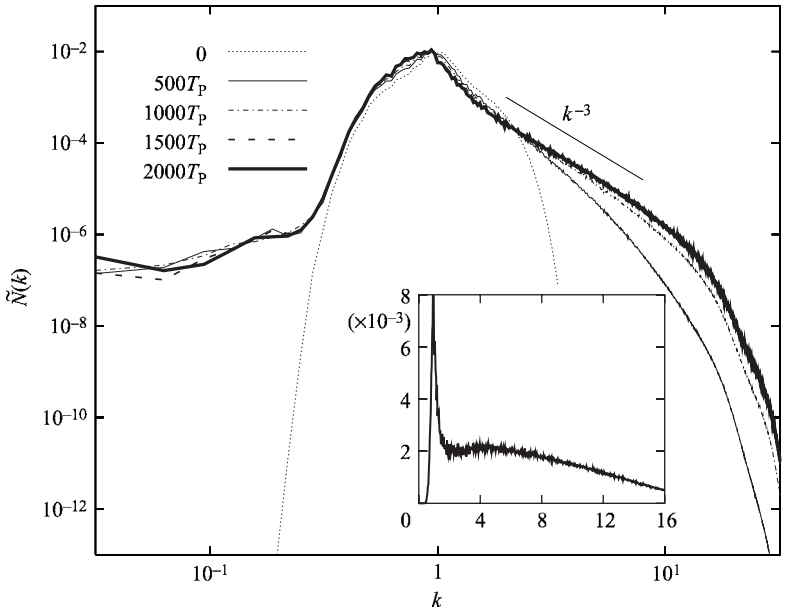

FIGURE 1. One-dimensional wave action spectrum. The inset shows the compensated spectrum $k^3\widetilde{N}(k)$ at $t = 2000T_P$. Both figures show that the spectrum has power-law behaviour quite close to -3, which is consistent with the prediction of the weak turbulence theory.

On the other hand, we should carefully choose the largest wavenumber, e.g. 1023/32 here, because large-wavenumber modes can make numerical simulations break down through collapsing waves, which is discussed in detail in § 4.

3. Results

First, we define the wave action spectrum as $N(\boldsymbol{k}) = |b(\boldsymbol{k})|^2$ in this paper. Although $N(\boldsymbol{k})$ is not exactly the same as $n(\boldsymbol{k})$, we can use $N(\boldsymbol{k})$ in place of $n(\boldsymbol{k})$ since the difference is negligible. We will discuss further in § 4. Moreover, in the discussion of the spectrum we use the directionally integrated spectrum, $\widetilde{N}(k) = \int \mathrm{d}\theta k N(\boldsymbol{k})$, where $k = |\boldsymbol{k}|$ and θ is the angle between $\boldsymbol{k}$ and the k_x-axis. We study the statistics at around $t = 2000T_P$ when the energy dissipation rate, $P = D(k)\omega(k)|b(\boldsymbol{k})|^2$, takes the maximum value, because the wave field at that time is fully developed. The maximum energy dissipation rate is approximately 10^{-8} and only 1.3% of the total wave action has been dissipated by $t = 2000T_P$.

Figure 1 shows the evolution of the directionally integrated wave action spectrum. At $t = 2000T_P$, it shows a clear power law in the range $1.7 \leqslant k \leqslant 7$ and its exponent obtained by the least-square method is -3.01 ± 0.01. The inset shows the compensated spectrum $k^3\widetilde{N}(k)$. It also shows a plateau from $k = 1.7$ to $k = 7$. The figures show that the power law is quite close to k^{-3}, which corresponds to the energy cascade from long waves to short waves predicted by the weak turbulence theory. It is noted that the directional integration adds one to the power-law exponents. Simultaneously, for small wavenumbers in the range $k \leqslant 0.25$ we can see another power-law behaviour. We consider that this shows the equipartition caused by the finite domain of this numerical simulation.

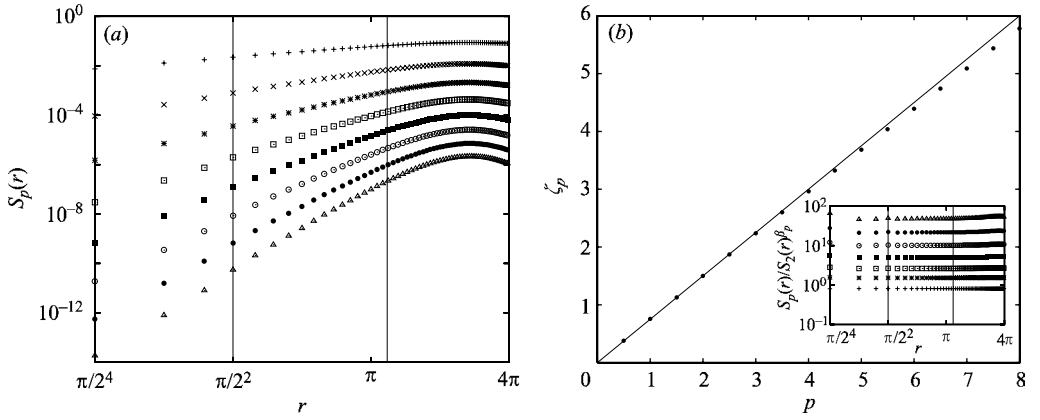

FIGURE 2. (a) pth-order structure functions of surface increments, $S_p(r)$. Curves are for $p = 1, 2, 3, \ldots, 8$ from top to bottom. (b) Scaling exponents of the structure functions, ζ_p, at $t = 2000T_P$. The solid line is the prediction of the weak turbulence theory. The scaling exponents are obtained by extended self-similarity fitted in the range $2\pi/7 \leqslant r \leqslant 2\pi/1.7$, indicated by the vertical lines in (a) and in the inset of (b). The error bars for the scaling exponents are much smaller than the point size. The inset of (b) shows the compensated structure functions $S_p(r)/S_2(r)^{\beta_p}$ except $p = 2$. Curves are for $p = 1, 3, 4, \ldots, 8$ from bottom to top.

Because of isotropy, two-point displacements in structure functions, $\boldsymbol{r}$, can be replaced by the modulus r. Figure 2 plots structure functions, $S_p(r)$, and their scaling exponents, ζ_p, up to the eighth order. Each function is averaged over four directions at $t = 2000T_P$ and all the exponents are obtained by the generalized scaling method called 'extended self-similarity' in research on fully developed Navier–Stokes turbulence (Benzi *et al.* 1996). In this paper, we plot $\zeta_p = 3\beta_p/2$, where β_p is the power-law exponent of $S_p(r)$ as functions of $S_2(r)$, that is $S_p(r) \propto S_2(r)^{\beta_p}$. Fitting is done in the range $2\pi/7 \leqslant r \leqslant 2\pi/1.7$, which corresponds with the power-law region of the wave action spectrum. We assumed $\zeta_2 = 3/2$ which is predicted by the weak turbulence theory because weak turbulence does not have exponents that can be derived analytically such as the Kolmogorov's four-fifth law in fully developed Navier–Stokes turbulence (Kolmogorov 1941) at this moment. While at small p the scaling exponents agree with the $3p/4$ that the weak turbulence theory predicts, at large p they deviate slightly downward from the prediction of the weak turbulence theory. However, the deviation in this system is much smaller than that in fully developed Navier–Stokes turbulence.

These power laws obtained by the direct numerical simulation show the success of the weak turbulence theory: the breakdown of the theory is quite weak. However, the deviation from the theory can be seen more distinctly in p.d.f.s of η and $\nabla_\perp^2\eta$. Figure 3 shows p.d.f.s taken with the wave fields at ten times extracted every $12.5T_P$ from $t = 1937.5T_P$ to $t = 2050T_P$ and normalized by the corresponding standard deviation.

The p.d.f. of η is close to the Gaussian distribution around the mean value and differs from it in the tail region. Its skewness and kurtosis are 1.45×10^{-1} and 3.12, respectively. The positive skewness is qualitatively described by Stokes waves that have steep tops and flat bottoms. The p.d.f. of $\nabla_\perp^2\eta$ represents the characteristics of the large wavenumbers and it displays the vertical asymmetry of the waves more clearly. The two-dimensional Laplacian $\nabla_\perp^2$ enlarges the small non-Gaussianity seen on the p.d.f. of η. It is greatly distorted from the Gaussian distribution, and its skewness and kurtosis are -7.92×10^{-1} and 4.92, respectively. In particular, it has an exponential

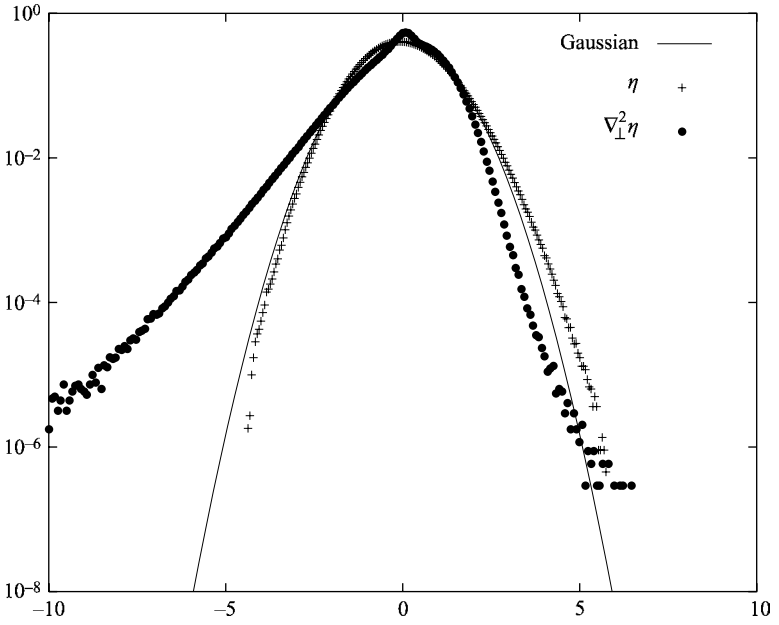

FIGURE 3. P.d.f.s of η and $\nabla_\perp^2\eta$. The p.d.f. of η differs marginally from the Gaussian distribution and that of $\nabla_\perp^2\eta$ is greatly distorted from the Gaussian distribution. The deviation from the Gaussian distribution is qualitatively described by a Stokes waves picture.

tail at negative values of $\nabla_\perp^2\eta$. This relatively large probability at negative values of $\nabla_\perp^2\eta$ and small probability at positive values of $\nabla_\perp^2\eta$ is also consistent with the picture of Stokes waves. In other words, the wave field consists of randomly distributed waves accompanied by bound waves like Stokes waves.

4. Discussion

With canonical variables $c(\boldsymbol{k})$ obtained by canonical transformation from $b(\boldsymbol{k})$ (Krasitskii 1994), the dynamic equations (2.2) are rewritten as

$$\frac{\partial c(\boldsymbol{k})}{\partial t} = -\mathrm{i}\omega(\boldsymbol{k})c(\boldsymbol{k}) - \mathrm{i}\int \mathrm{d}\boldsymbol{k}_{123}\delta^{k}_{0+1-2-3}T_{0,1,2,3}c^*(\boldsymbol{k}_1)c(\boldsymbol{k}_2)c(\boldsymbol{k}_3). \tag{4.1}$$

This equation has no three-wave interaction terms. The weak turbulence theory is applied not to $b(\boldsymbol{k})$ but to $c(\boldsymbol{k})$ and wave action should be defined as $n(\boldsymbol{k}) = \langle |c(\boldsymbol{k})|^2 \rangle$. Transformation between $b(\boldsymbol{k})$ and $c(\boldsymbol{k})$ is impossible though, even numerically, because the transformation needs many convolutions to be calculated. However, the difference is of the order of the square of the wave action and appears only in large-wavenumber regions (see also Krasitskii 1994). Therefore we can regard the difference between $b(\boldsymbol{k})$ and $c(\boldsymbol{k})$ as sufficiently small in our numerical simulations.

Milder (1990) states that the truncation of the Hamiltonian to finite orders causes higher-order imperfections and that the unstable wavenumber decreases in proportion to the surface slope. However, the truncation contains more sensitive problems. We expand $\exp(|\boldsymbol{k}|z)$ into $1 + |\boldsymbol{k}|z + (|\boldsymbol{k}|z)^2/2 + \cdots$ at the water surface. In this process we implicitly assume that higher-order terms are much smaller than lower-order terms, that is, $|b(\boldsymbol{k}_1)| \gg |b(\boldsymbol{k}_2)b(\boldsymbol{k}_3)| \gg |b(\boldsymbol{k}_4)b(\boldsymbol{k}_5)b(\boldsymbol{k}_6)| \gg \cdots$ for arbitrary combinations of the $\boldsymbol{k}_i$. In fact, this assumption does not always hold because of the power-law

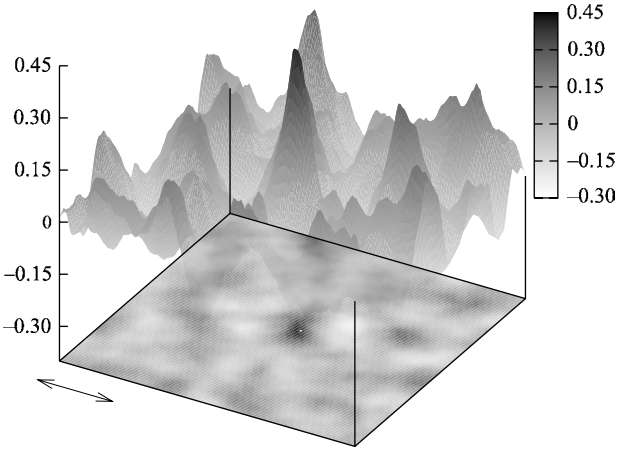

FIGURE 4. A collapsing wave $0.01T_P$ before the breakdown of the computation. The height of the collapsing wave located in the centre of the figure is approximately six times as large as the standard deviation for the surface elevation. The arrow shows the wavelength of the peak wavenumber and $(1/8)^2$ of the whole computational domain is shown.

nature of the spectrum. Here the locality of interactions is required. The locality of interactions means that energy is transferred among the wavenumbers of which norms and wave action are of the same order. The locality that is also assumed by cascading models has not been clarified yet in spite of its importance.

We carried out another simulation with higher resolution in space, where the largest wavenumber is 2047/32. The time steps Δt are variable. The coefficient of the dissipation term ν is 8.04×10^{-28}, which is determined so that the dissipation rate of the wave action at the largest wavenumbers has the same value as that in the previous simulation assuming $\widetilde{N}(k) \propto k^{-3}$. The energy dissipation rate P is larger in this simulation than that in the previous one. Other parameters are set to the same value as in the previous simulation. Despite the larger energy dissipation rate than in the previous simulation, the numerical computation breaks down. This indicates that mechanisms of wave interactions that do not contribute to the energy cascade are dominant in the large-wavenumber region. Figure 4 displays the wave field just before the breakdown of the computation, when a local point-like collapse appears. It is probably inappropriate to apply the expansion of $\exp(|\boldsymbol{k}|z)$ and the truncation of the Hamiltonian to wave fields with large $|\boldsymbol{k}|z$ such as collapses. Hence, high-resolution simulations are necessary to clarify the behaviour of these collapsing waves in a system including the higher-order terms or in a three-dimensional free surface system without truncation.

Newell, Nazarenko & Biven (2001) showed that intermittent phenomena that originate in coherent structures like whitecaps occur and the weak turbulence theory is violated at large wavenumbers. If we apply their theory to our numerical computation, the intermittent phenomena occur around $k \sim 10^5$. Nevertheless, we found strong dynamical structures such as collapses in our simulation in which the largest wavenumber is only $2047/32 \sim 64$. The difference is that their estimation is based on the kinetic equation (1.1) derived via the weak turbulence theory and our simulation is based on the dynamic equations (2.4). Namely, breakdown of the weak turbulence theory occurs at relatively small wavenumbers, although the overall statistics for the wave field with a limited inertial range is described by the theory.

Intermittency in this system, which is deviation from the prediction of the weak turbulence theory, consists of two types. One is the characteristics of the bound waves and the other comes from the dynamical structures localized in time and space of huge waves such as collapsing waves. The former is seen everywhere in the wave field and its effect is not large. On the other hand, the latter is spatio-temporal intermittency and is rarely seen in statistics, unlike fully developed Navier–Stokes turbulence. However, this spatio-temporal intermittency, which is linked to discontinuity in mathematics and freak waves in oceanography, has extremely serious effects on the wave field. Janssen (2003) studied large-scale freak waves induced by the sideband instability in the narrow-band system governed by the nonlinear Schrödinger equation. We will clarify the relation between large waves caused by the sideband instability and the spatio-temporal intermittency in the broad-band water wave system in future work.

5. Conclusion

In this paper, we perform direct numerical simulations of gravity waves on infinite-depth water. This calculation is based on the dynamic equations without any statistical approximations instead of the kinetic equation derived with the random phase approximation.

We reproduced the power-law behaviour of the wave action spectrum for an isotropic initial spectrum. We also obtained the power-law range of the structure functions of the displacement of the wave surface elevation. These power laws agree quite well with the prediction of the weak turbulence theory and indicate the success of the theory. In addition, we show that p.d.f.s of the wave field are skewed by bound waves.

However, we found evidence of rare events such as collapsing waves that are the origin of spatio-temporal intermittency and outside the concept of weak turbulence theory. Intermittency in this system comes from the dynamical mechanism and thus it is qualitatively different from that in the fully developed turbulence described by the Navier–Stokes equation. From both practical and mathematical viewpoints investigation of these spatio-temporal intermittent structures is important.

I would like to thank to Mitsuhiro Tanaka and Sadayoshi Toh for continuous encouragement and valuable discussion. This work is partially supported by the Grand-Aid for Scientific Research from the Ministry of Education, Culture, Sports and Technology of Japan (No. 15540419). Numerical computation in this work was carried out at Yukawa Institute of Kyoto University and Information Synergy Center of Tohoku University.

REFERENCES

Benzi, R., Biferale, L., Ciliberto, S., Struglia, M. & Tripiccione, R. 1996 Generalized scaling in fully developed turbulence. *Physica* D **96**, 162–181.

Cai, D. & McLaughlin, D. W. 2000 Chaotic and turbulent behavior of unstable one-dimensional nonlinear dispersive waves. *J. Math. Phys.* **41**, 4125–4153.

Dias, F., Guyenne, P. & Zakharov, V. E. 2001 Kolmogorov spectra of weak turbulence in media with two types of interacting waves. *Phys. Lett.* A **291**, 139–145.

Janssen, P. A. E. M. 2003 Nonlinear four-wave interactions and freak waves. *J. Phys. Oceanogr.* **33**, 863–884.

Kartashova, E. 1998 Wave resonances in systems with discrete spectra. In *Nonlinear Waves and Weak Turbulence* (ed. V. Zakharov), pp. 95–129. Am. Math. Soc.

Kolmogorov, A. 1941 Dissipation of energy in the locally isotropic turbulence. *Dokl. Akad. Nauk. SSSR* **434**, 16–18.

Komen, G., Cavaleri, L., Donelan, M., Hasselmann, K., Hasselmann, S. & Janssen, P. 1994 *Dynamics and Modelling of Ocean Waves*. Cambridge University Press.

Krasitskii, V. 1994 On reduced equation in the Hamiltonian theory of weakly nonlinear surface waves. *J. Fluid Mech.* **272**, 1–20.

Milder, D. M. 1990 The effects of truncation on surface-wave Hamiltonian. *J. Fluid Mech.* **216**, 249–262.

Newell, A. C., Nazarenko, S. & Biven, L. 2001 Wave turbulence and intermittency. *Physica* D **152–153**, 520–550.

Onorato, M., Osborne, A. R., Serio, M., Resio, D., Pushkarev, A., Zakharov, V. E. & Brandini, C. 2002 Freely decaying weak turbulence for sea surface gravity waves. *Phys. Rev. Lett.* **89**, 144501.

Polnikov, V. 1994 Numerical modelling of flux spectra formation for surface gravity waves. *J. Fluid Mech.* **278**, 289–296.

Polnikov, V. 2001 Numerical modeling of the constant flux spectra for surface gravity waves in a case of angular anisotropy. *Wave Motion* **33**, 271–282.

Pushkarev, A. & Zakharov, V. 2000 Turbulence of capillary waves – theory and numerical simulation. *Physica* D **135**, 98–116.

Tanaka, M. 2001 Verification of Hasselmann's energy transfer among surface gravity waves by direct numerical simulations of primitive equations. *J. Fluid Mech.* **444**, 199–221.

Tanaka, M. & Yokoyama, N. 2004 Effects of discretization of the spectrum in water-wave turbulence. *Fluid Dyn. Res.* (to appear).

Zakharov, V. 1968 Stability of periodic waves of finite amplitude on the surface of a deep fluid. *J. Appl. Mech. Tech. Phys.* **2**, 190–194.

Zakharov, V. & Filonenko, N. 1967 Energy spectrum for stochastic oscillations of the surface of a liquid. *Sov. Phys. Dokl.* **10**, 881–883.

Zakharov, V. E., Vasilyev, O. A. & Dyachenko, A. I. 2001 Kolmogorov spectra in one-dimensional weak turbulence. *JETP Lett.* **73**, 63–65.